ISSN 0957-4484

NANOTECHNOLOGY

VOLUME 20 NUMBER 18 6 MAY 2009

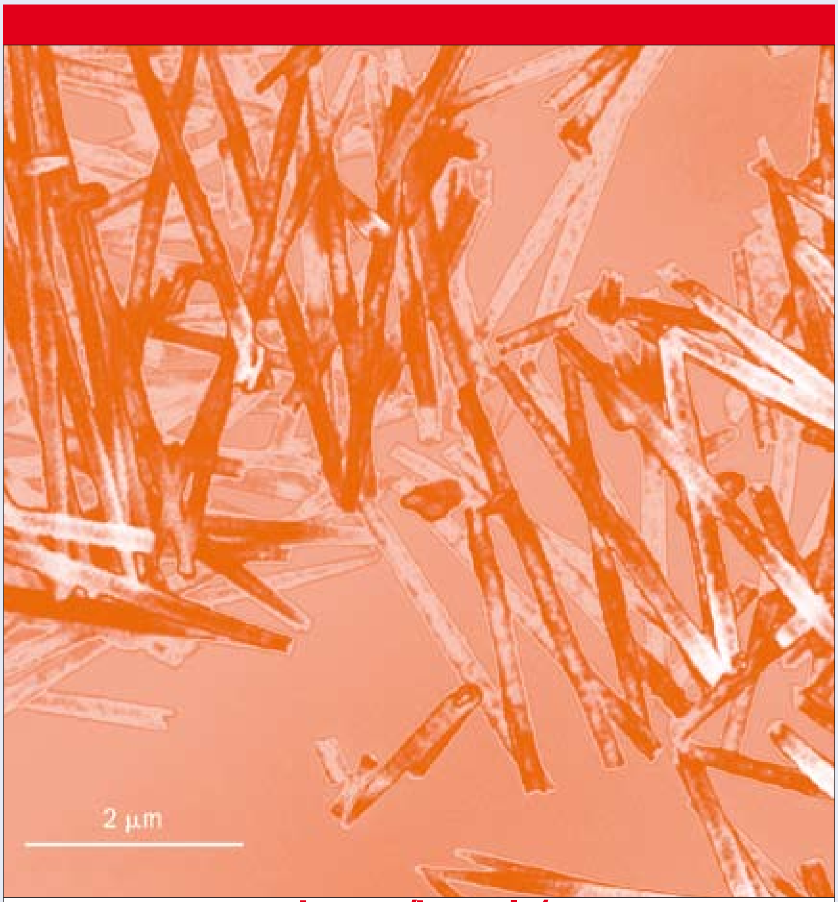

www.iop.org/journals/nano

Featured article

Size-controlled electrochemical synthesis and properties of SnO_2 nanotubes

M Lai, J-H Lim, S Mubeen, Y Rheem, A Mulchandani, M A Deshusses and N V Myung

IOP Publishing

Nanotechnology **20** (2009) 185602 (6pp) doi:10.1088/0957-4484/20/18/185602

Size-controlled electrochemical synthesis and properties of SnO_2 nanotubes

Min Lai[1,2], **Jae-Hong Lim**[2], **Syed Mubeen**[2], **Youngwoo Rheem**[2],
Ashok Mulchandani[2], **Marc A Deshusses**[3] **and Nosang V Myung**[2,4]

[1] School of Mathematics and Physics, Nanjing University of Information Science and
Technology, Nanjing, 210044, People's Republic of China
[2] Department of Chemical and Environmental Engineering, University of California-Riverside,
Riverside, CA 92521, USA
[3] Department of Civil and Environmental Engineering, Duke University, Box 90287, Durham,
NC 27708, USA

E-mail: myung@engr.ucr.edu

Received 2 February 2009, in final form 9 March 2009
Published 15 April 2009
Online at stacks.iop.org/Nano/20/185602

Abstract

SnO_2 nanotubes with controlled diameter and length were synthesized using an electrochemical method at room temperature. The length and wall thickness of the nanotubes increased monotonically with the deposition time and the diameter of the nanotubes was altered by varying the pore size of the scaffolds. Post-annealing at 400 °C in dry air significantly improved the crystallinity while maintaining the nanotube structure. The temperature-dependent photoluminescence spectra indicated an activation energy of 58 meV for emission centered at 410 nm. The temperature-dependent electrical resistance revealed that the dominant electrical conduction mechanism alters from the ionization of the main donor centers to impurity scattering as the temperature decreases. The electrical conductance of 200 nm diameter nanotubes increased to 33 times the original value upon UV illumination at 254 nm.

1. Introduction

Tin dioxide (SnO_2) is a n-type semiconductor with a large band gap ($E_g = 3.6$ eV at 300 K) which shows promise for a number of applications including transparent conductors and solid state gas sensors. For example, owing to its high light-transparency in the visible range and low electrical resistance, tin dioxide has been used widely as transparent conductors in dye sensitized solar cells (DSSCs) and in light emitting diodes (LEDs) [1–3].

Recently, one-dimensional (1D) tin dioxide nanostructures have attracted intensive interest due to their size-dependent properties. SnO_2 nanowire-based devices were fabricated to use as optoelectronics, which showed a different electrical conductance upon exposure to ultraviolet (UV) irradiation [4]. In addition, 1D SnO_2 nanostructures were shown to be suitable for the detection of oxidative and reductive gases [5]. The good sensing properties of 1D SnO_2 nanostructures compared to thick films and bulk counterparts has been attributed to the enhanced surface-to-bulk ratio of the nanostructures and the comparable diameters of nanostructures with respect to the width of the surface space charge region (SCR) [5f].

A variety of physical and chemical methods have been developed to synthesize 1D SnO_2 nanostructures. High-frequency inductive heating [6], chemical vapor deposition (CVD) [4a, 7], high-temperature thermal evaporation [8], laser ablation [4b], thermal decomposition [9], molten salt synthesis [10] have been used to produce single-crystal or polycrystalline SnO_2 nanorods [10], nanowires [4a, 7b, 8b, 9], nanotubes [7a, 8b, 6], and nanoribbons [8]. These methods require rigid conditions and expensive tin precursors. 1D SnO_2 nanostructures have also been prepared by hydrothermal processes [11] and template-directed electrodeposition [12]. In order to fabricate tin oxide nanostructures-based electronics and sensors using conventional optical lithography, the length of nanostructures needs to be in a few microns. However, the reported tin dioxide nanostructures mainly focused on the materials properties and researchers did not optimize the synthesis conditions to fabricate a high aspect ratio nanostructures.

---

[4] Address for correspondence: Department of Chemical and Environmental Engineering at University of California-Riverside, Bourns Hall B353, 900 University Avenue, Riverside, CA 92521, USA.

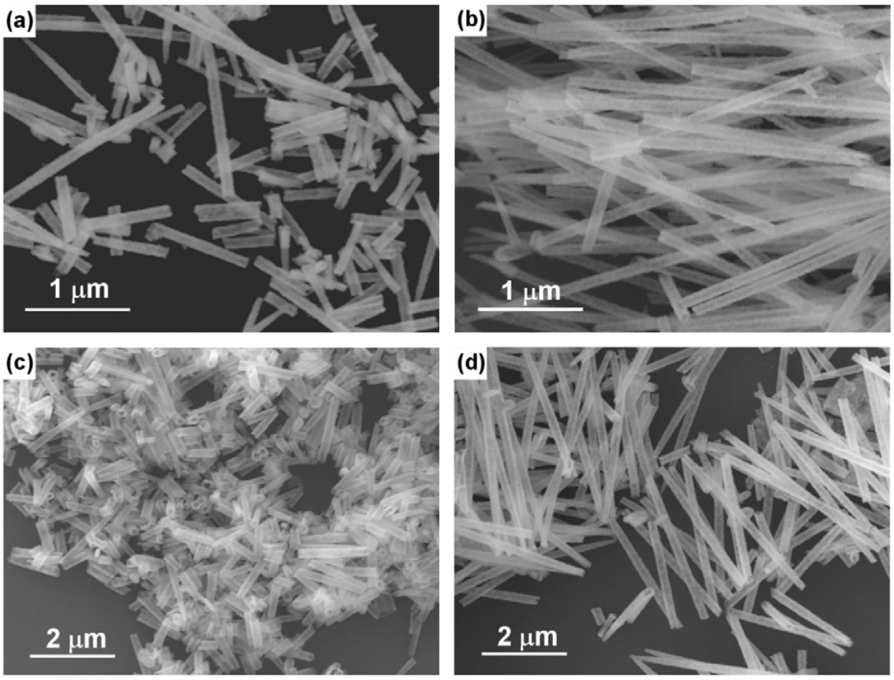

Figure 1. FE-SEM images of as-synthesized SnO_2 nanotubes using 50 nm ((a) and (b)) and 100 nm ((c) and (d)) polycarbonate membranes with deposition time of 2 h ((a) and (c)) and 12 h ((b) and (d)).

In this work, we optimized deposition conditions to demonstrate the size-controlled electrochemical synthesis of SnO_2 nanotubes. The aspect ratio and diameter of nanotubes was controlled by adjusting deposition time and template pore diameter. The high aspect ratio long nanotubes were achieved by longer deposition time (12 h) followed by mild washing steps. The morphology and crystal structure of synthesized SnO_2 nanotubes were examined using scanning electron microscopy (SEM), high-resolution transmission electron microscopy (HR-TEM), and selective-area diffraction pattern (SAED). Temperature-dependent electrical resistance and photoluminescence (PL) spectra were measured to determine electrical, optical, and optoelectronic properties of synthesized SnO_2 nanotubes.

2. Experimental details

SnO_2 nanotubes were synthesized by template-directed electrodeposition using nuclear track etch polycarbonate membranes (Whatman Nuclepore®) with a nominal pore diameter of 50 or 100 nm. The rated thickness and pore density were 6 μm and 6 × 10^8 pores cm^{-2}, respectively. One side of the polycarbonate membrane was first coated with 500 nm thick layer of gold by sputtering, to create a seed layer. The electrical contact was made to the membrane working electrode using conductive copper tape. The resultant template was placed in an electrolyte cell such that an area of 1 cm^2 was exposed to the electrolyte. Platinum gauze was used as the counter electrode and Ag/AgCl (3 M KCl) electrode served as the reference electrode. Electrochemical synthesis was performed under potentiostatic mode using a VMP2 multichannel potentio/galvanostat. The electrolyte consisted of 20 mM tin chloride, 0.1 M sodium nitrate and 75 mM nitric acid in Nanopure (>18 MΩ cm^{-1}) water. SnO_2 was deposited in the templates using a fixed potential of -0.4 V (versus Ag/AgCl) with varying deposition times. Following deposition, the gold seed layer used as the working electrode was mechanically removed and the membrane was rinsed in deionized water. The nanotubes were released by dissolving the polycarbonate membrane in dichloromethane. The suspension was centrifuged and the nanotubes were washed three times with dichloromethane and finally suspended in 0.5 ml isopropanol. The resultant SnO_2 nanotubes were annealed in air at 400 °C for 4 h to investigate the effect of annealing on the crystal structure of the nanotubes.

Field-emission scanning electron microscope (FE-SEM) images were obtained using a Philips XL30 FEG SEM microscope operated at 15 kV. Transmission electron microscope (TEM), high-resolution TEM (HR-TEM) images and selected-area electron diffraction (SAED) patterns were recorded on a FEI-Philips CM300 microscope operated at 200 kV. PL measurements were performed using a He–Cd laser centered at 325 nm as the excitation source in the temperature range $10\ K \leqslant T \leqslant 300\ K$. The electrodes for the temperature-dependent resistance and photocurrent measurements were microfabricated by coating (100) oriented silicon wafers with 1 μm thick SiO_2 film by CVD, photo lithographically defining the electrode area, evaporating a Cr adhesion layer and a 300 nm thick Au layer and finally defining the electrodes using lift-off techniques. The gap distance between electrodes was fixed at 3 μm. SnO_2 nanotubes were assembled on the electrodes by AC dielectrophoretic alignment with a peak-to-peak voltage of 20 V and frequency of 1 MHz, using aqueous suspensions. Temperature-dependence of electrical resistance

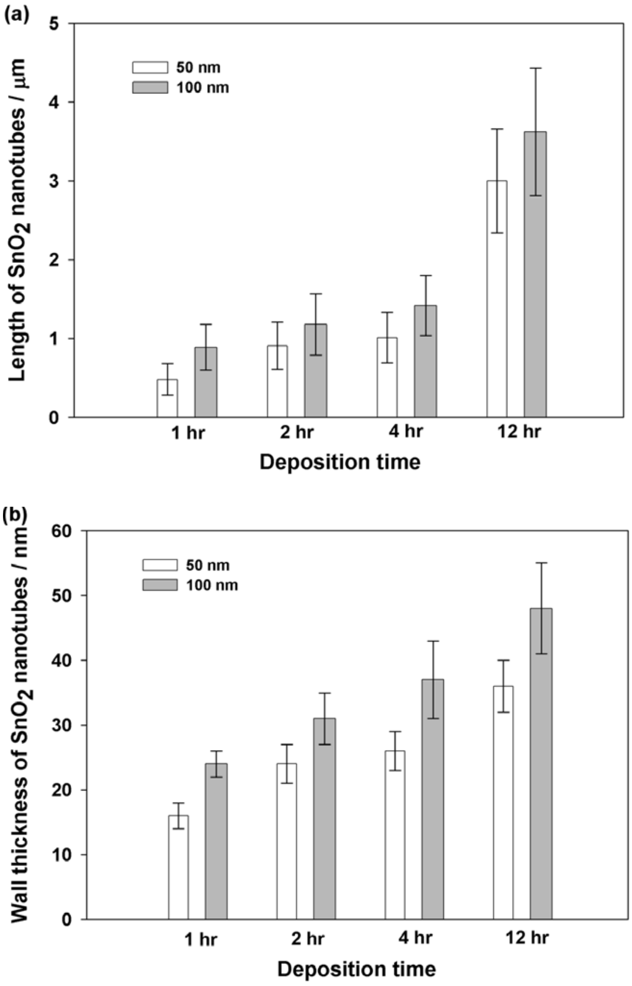

Figure 2. Histograms of (a) length and (b) wall thickness of electrochemically synthesized SnO_2 nanotubes. The error bars denote standard deviations.

was studied using a Keithley 236 Source-Measure Unit and a Cryogenic cooling system. Photocurrent measurements at room temperature were performed using a UV lamp of 254 nm in wavelength with a power density of 0.25 mW cm^{-2}.

3. Results and discussion

The electrochemical synthesis of tin dioxide is a two step process [13]: (i) in acidic environment, nitrate ions are electrochemically reduced at the surface of the working electrode, resulting in an increase in local pH in the vicinity of the electrode (equation (1)); (ii) the increase in the local pH leads to the precipitation of tin ions as tin dioxide (equations (2) and (3)).

$$NO_3^- + 2H^+ + 2e^- \rightarrow NO_2^- + H_2O \quad E^{O} = +0.934\ \mathrm{V(SHE)} \tag{1}$$

$$Sn^{4+} + 4H_2O \rightarrow Sn(OH)_4 + 4H^+ \tag{2}$$

$$Sn(OH)_4 \rightarrow SnO_2(S) + 2H_2O \tag{3}$$

$$Sn^{4+} + 2NO_3^- + 4e^- \rightarrow SnO_2(S) + 2NO_2^-. \tag{4}$$

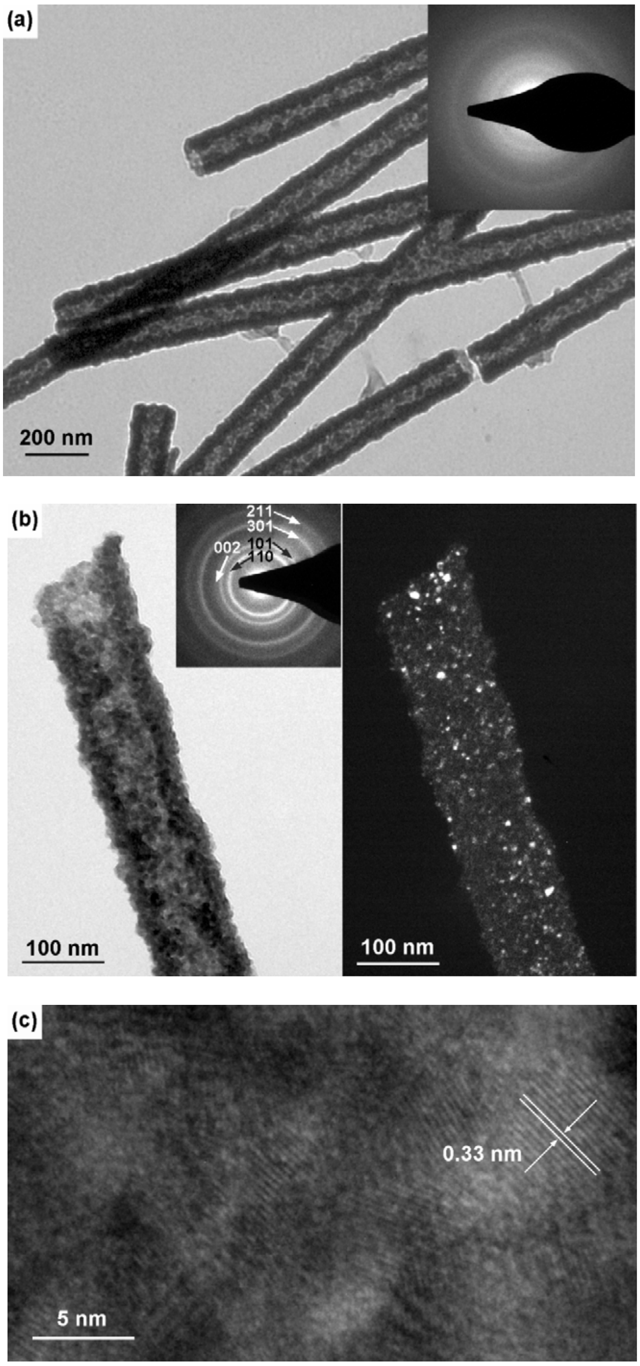

Figure 3. (a) BF-TEM image of as-prepared SnO_2 nanotubes electrodeposited in 50 nm polycarbonate membranes for 12 h. Inset is the corresponding SAED pattern. (b) BF-(left) and DF-(right) TEM images of annealed SnO_2 nanotubes. Insets are the corresponding SAED pattern. (c) HR-TEM image of the SnO_2 nanotube in (b).

FE-SEM images of SnO_2 nanotubes prepared in 50 and 100 nm track-etched polycarbonate membranes with different deposition times are displayed in figure 1. The formation of nanotubes rather than nanowires was attributed to preferential precipitation on the membrane walls leaving the center of the tubes hollow [12]. The actual diameters of SnO_2 nanotubes prepared in membranes with the nominal diameters of 50 nm

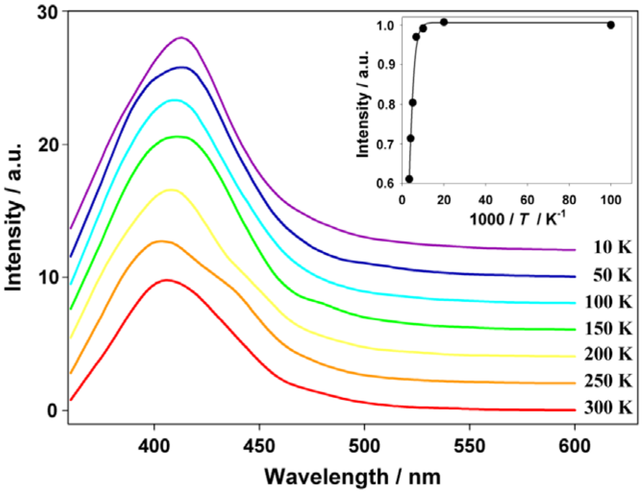

Figure 4. Temperature-dependent photoluminescence spectra of annealed SnO_2 nanotubes. Inset is the plot of the integral intensity versus $1000/T$ and the solid line is the first-order exponential fitting. (This figure is in colour only in the electronic version)

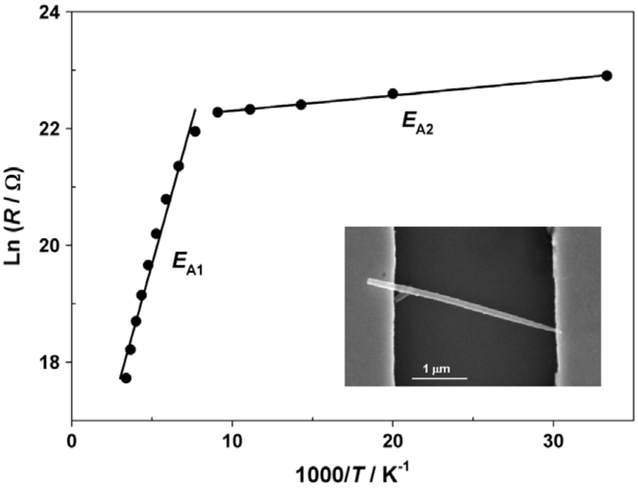

Figure 5. Arrhenius plot of temperature-dependent resistance of annealed SnO_2 nanotubes. E_{A1} and E_{A2} represent the activation energy obtained from the two different temperature regions. Inset is the SEM image of the single SnO_2 nanotube aligned on gold electrodes by AC dielectrophoretic alignment.

and 100 nm were 103 ± 13 and 200 ± 29 nm, respectively. The difference between nominal pore size of membrane and diameter of nanotubes can be attributed to cigar shaped pore structure and swelling of the pores of membrane during deposition. The histograms in figures 2(a) and (b) show the effect of increasing deposition times on the length and wall thickness of the SnO_2 nanotubes. In general, the length and wall thickness monotonically increased with increasing deposition time. The growth rate and wall thickness of SnO_2 nanotubes depended on the pore size, with larger pore size leading to faster deposition rates and thicker walls. This might be attributed to faster diffusion rate of nitrate ions in larger pore. Large aspect ratio (up to 40) nanotubes were achieved by depositing SnO_2 for 12 h. Greater aspect ratio nanotubes can be synthesized if the thickness of scaffolds is larger and the deposition time is increased. The tubular structure was confirmed by TEM imaging (see figure 3(a)). Examination of the TEM image reveals that the wall thickness is uniform. The corresponding SAED pattern (inset figure 3(a)) indicates that the as-prepared SnO_2 nanotubes had a poor crystallinity.

In order to improve the crystallinity of the nanotubes, they were annealed in air at 400 °C for 4 h. The bright field (BF)-TEM image indicated that the tubular structure was maintained after annealing (figure 3(b), left). The corresponding SAED pattern (inset figure 3(b)), and dark field (DF)-TEM image show that the crystallinity of SnO_2 nanotubes was markedly improved (figure 3(b) inset). The SAED pattern is consistent with polycrystalline rutile SnO_2 structures. Figure 3(c) shows the HR-TEM image of annealed SnO_2 nanotubes and the distance of the marked fringes which is consistent with interplanar spacing of the rutile $SnO_2\{110\}$ planes.

The temperature-dependent PL spectra of annealed SnO_2 nanotubes are shown in figure 4. The broad emission centered at ~410 nm (3.02 eV) can be attributed to all luminescent centers, such as nanocrystals and defects in the sample [14]. The temperature-dependence of the (eV) PL intensity can be expressed by a thermal activation model [15], where E_A is the activation energy, $I(T)$ and I_o are PL intensity at temperature T and absolute zero temperature, A is a constant and k_B is the Boltzmann constant.

$$I(T) = I_o/(1 + A\exp(E_A/k_BT)). \tag{5}$$

By fitting the experimental data (figure 4 inset) using equation (5), an activation energy $E_A = 58 \pm 7$ meV is obtained for the nonradiative mechanisms responsible for quenching the luminescence. The temperature-dependence of the electrical resistance, for semiconducting materials can be given by

$$R(T) = R_o\exp(E_A/k_BT) \tag{6}$$

where T, k_B, E_A and R_o are the temperature, the Boltzmann constant, the activation energy and the pre-exponential factor, respectively. The Arrhenius plot of temperature-dependent resistance of annealed SnO_2 nanotubes is shown in figure 5. The resistivity of the SnO_2 nanotubes is approximately 0.36 Ω cm in air at room temperature. Two linear regions are observed on the plot. By linear fitting in those two regions, two activation energy values, 84 ± 6 meV (E_{A1}) and 2.3 ± 0.1 meV (E_{A2}), are obtained for temperatures above and below 130 K. The activation energy, E_{A1}, observed experimentally above 130 K is attributed to the ionization energy of the main donor centers [16]. At temperatures below 130 K, the nanotubes resistance is weakly dependent on the temperature which indicates that a different conduction mechanism is dominant. Modest variations of the resistance at low temperatures have also been observed for CdTe thin films [17] and nanowires [18] and ZnO [16] and GaN [19] nanowires. The experimental results of the figures can be explained by the fact that the electrical conduction comes from impurity scattering [17]. The transition temperature of the impurity band conduction is approximately 130 K. Such impurity states can be associated to defects located either in the bulk or on the surface of the SnO_2 nanotubes.

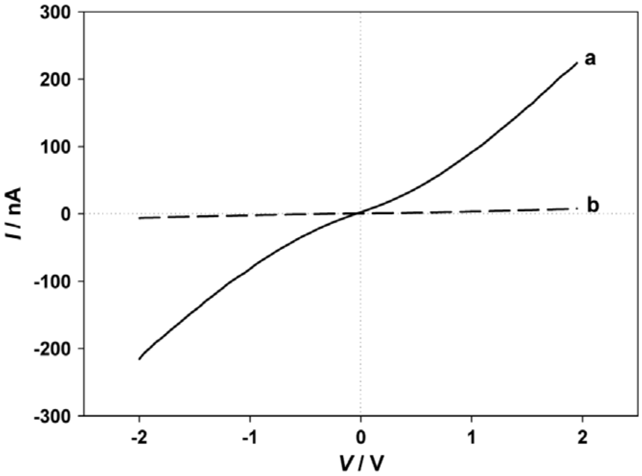

Figure 6. I–V characteristics of annealed SnO_2 nanotube in the presence (a) and absence (b) of UV illumination (254 nm).

The optoelectronic response of the SnO_2 nanotubes was investigated in air using UV light with a wavelength of 254 nm. Figure 6 shows two I–V curves for the SnO_2 nanotubes with UV light on and off, respectively. When exposed to UV light, the nanotube conductance increased on average 33 fold ($N = 6$ devices, ranging from 26 to 36 fold). Two major mechanisms were likely involved in the conductance rise. First, electrons were directly excited from the valence band into the conduction band by the UV light of 254 nm in wavelength which corresponds to 4.9 eV. This led to the increase of the number of free carriers within the nanotubes and, hence, the conduction enhancement. Second, the UV light triggered the photodesorption of oxygen and moisture on the nanotube surface, which resulted in the decrease of the width of the electron depletion layer near the surface [4, 20].

4. Conclusion

In summary, it has been shown that large aspect ratio SnO_2 nanotubes can be electrochemical synthesized in porous polycarbonate membranes. The length and wall thickness of the nanotubes monotonically depended on the deposition time at fixed potential. The diameter of nanotubes can be varied by selecting membranes with different pore sizes. The temperature-dependent PL spectra revealed an activation energy of 58 meV for emission centered at 410 nm. The temperature-dependence of electrical resistance was investigated and two dominant mechanisms were attributed to the electrical conduction above and below 130 K, respectively. The study of photoconduction properties based on our devices showed that the conductance increased 33 times with 254 nm UV illumination. The simple synthesis method associated with large aspect ratio (up to 40) of SnO_2 nanotubes with controlled diameter paves the way for exciting applications in 1D nanostructure-based devices.

Acknowledgments

This material is based on research sponsored by the National Institute of Environmental Health Sciences under agreement number (grant No. U01ES016026). The United States government is authorized to reproduce and distribute reprints for government purposes, not withstanding any copyright notation thereon.

References

[1a] Laitinen H A, Vincent C A and Bednarski T M 1968 *J. Electrochem. Soc.* **115** 1024
[1b] Elliot D, Zellmer D L and Laitinen H A 1970 *J. Electrochem. Soc.* **117** 1345
[2] Grätzel M 2001 *Nature* **414** 338
[3] Ho P K H, Kim J S, Burroughes J H, Becker H, Li S F Y, Brown T M, Cacialli F and Friend R H 2000 *Nature* **404** 481
[4a] Mathur S, Barth S, Shen H, Pyun J-C and Werner U 2005 *Small* **1** 713
[4b] Liu Z, Zhang D, Han S, Li C, Tang T, Jin W, Liu X, Lei B and Zhou C 2003 *Adv. Mater.* **15** 1754
[4c] Law M, Kind H, Messer B, Kim F and Yang P D 2002 *Angew. Chem. Int. Edn* **41** 2405
[5a] Kolmakov A, Zhang Y, Cheng G and Moskovits M 2003 *Adv. Mater.* **15** 997
[5b] Wang Y, Jiang X and Xia Y 2003 *J. Am. Chem. Soc.* **125** 16176
[5c] Zhang Y, Kolmakov A, Chretien S, Metiu H and Moskovits M 2004 *Nano Lett.* **4** 403
[5d] Comini E, Faglia G, Sberveglieri G, Calestani D, Zanotti L and Zha M 2005 *Sensors Actuators* B **111** 2
[5e] Yu C, Hao Q, Saha S, Shi L, Kong X and Wang Z L 2005 *Appl. Phys. Lett.* **86** 063101
[5f] Sysoev V V, Button B K, Wepsiec K, Dmitriev S and Kolmakov A 2006 *Nano Lett.* **6** 1584
[6] Li Z, Wang H, Liu P, Zhao B and Zhang Y 2009 *Appl. Surf. Sci.* **255** 4470
[7a] Liu Y and Liu M 2005 *Adv. Funct. Mater.* **15** 57
[7b] Ma Y-J, Zhou F, Lu L and Zhang Z 2004 *Solid State Commun.* **130** 313
[8a] Dai Z R, Pan Z W and Wang Z L 2001 *Solid State Commun.* **118** 351
[8b] Dai Z R, Gole J L, Stout J D and Wang Z L 2002 *J. Phys. Chem.* B **106** 1274
[9a] Xu C, Xu G, Liu Y, Zhao X and Wang G 2002 *Scr. Mater.* **46** 789
[9b] Wang Y, Jiang X and Xia Y 2003 *J. Am. Chem. Soc.* **125** 16176
[9c] Jiang X, Wang Y, Herricks T and Xia Y 2004 *J. Mater. Chem.* **14** 695
[10a] Liu Y, Zheng C, Wang W, Yin C and Wang G 2001 *Adv. Mater.* **13** 1883
[10b] Liu Y, Zheng C, Wang W, Zhan Y and Wang G 2001 *J. Cryst. Growth* **233** 8
[11a] Zhang D-F, Sun L-D, Yin J-L and Yan C-H 2003 *Adv. Mater.* **15** 1022
[11b] Vayssieres L and Graetzel M 2004 *Angew. Chem. Int. Edn* **43** 3666
[12] Lai M, Martinez J A G, Grätzel M and Riley D J 2006 *J. Mater. Chem.* **16** 2843
[13] Chang S T, Leu I C and Hon M H 2002 *Electrochem. Solid-State Lett.* **5** C71
[14a] Kim T W, Lee D U and Yoon Y S 2000 *J. Appl. Phys.* **88** 3759
[14b] Wang B, Yang Y H, Wang C X, Xu N S and Yang G W 2005 *J. Appl. Phys.* **98** 124303
[15] Jiang D S, Jung H and Ploog K 1988 *J. Appl. Phys.* **64** 1371
[16] Tazlaoanu C, Ion L, Enculescu I, Sima M, Enculescu M, Matei E, Neumann R, Bazavan R, Bazavan D and Antohe S 2008 *Physica* E **40** 2504

[17] Moesslein J, Lopez-Otero A, Fehrenbruch A, Kim D and Bube R H 1993 *J. Appl. Phys.* **73** 8359

[18] Kum M C, Yoo B Y, Rheem Y W, Bozhilov K N, Chen W, Mulchandani A and Myung N V 2008 *Nanotechnology* **19** 325711

[19a] Simpkins B S, Pehrsson P E and Laracuente A R 2006 *Appl. Phys. Lett.* **88** 072111

[19b] Motayed A, Davydov A V, Mohammad S N and Melngailis J 2008 *J. Appl. Phys.* **104** 024302

[20] Yamazoe N, Fuchigami J, Kishikawa M and Seiyama T 1978 *Surf. Sci.* **86** 335